


## Electronic structure of cuprate-nickelate infinite-layer heterostructure

Dachuan Chen(陈大川), Paul Worm, Liang Si(司良), Chunxiao Zhang(张春小), Fenglin Deng(邓凤麟),Peiheng Jiang(蒋沛恒), and Zhicheng Zhong(钟志诚)

**Citation:**Chin. Phys. B, 2023, 32 (**8**): 087105. DOI: 10.1088/1674-1056/acd368
Journal homepage: http://cpb.iphy.ac.cn; http://iopscience.iop.org/cpb

**What follows is a list of articles you may be interested in**

---

## Single crystal growth and electronic structure of Rh-doped $Sr_3Ir_2O_7$

Bingqian Wang(王冰倩), Shuting Peng(彭舒婷), Zhipeng Ou(欧志鹏), Yuchen Wang(王宇晨), Muhammad Waqas, Yang Luo(罗洋), Zhiyuan Wei(魏志远), Linwei Huai(淮琳崴),Jianchang Shen(沈建昌), Yu Miao(缪宇), Xiupeng Sun(孙秀鹏), Yuewei Yin(殷月伟), and Junfeng He(何俊峰)

Chin. Phys. B, 2023, 32 (**8**): 087108. DOI: 10.1088/1674-1056/acd7d5

## Electronic structure of cuprate-nickelate infinite-layer heterostructure

Dachuan Chen(陈大川), Paul Worm, Liang Si(司良), Chunxiao Zhang(张春小), Fenglin Deng(邓凤麟),Peiheng Jiang(蒋沛恒), and Zhicheng Zhong(钟志诚)

Chin. Phys. B, 2023, 32 (**8**): 087105. DOI: 10.1088/1674-1056/acd368

## Topological properties of tetratomic Su-Schrieffer-Heeger chains with hierarchical long-range hopping

Guan-Qiang Li(李冠强), Bo-Han Wang(王博涵), Jing-Yu Tang(唐劲羽), Ping Peng(彭娉), and Liang-Wei Dong(董亮伟)

Chin. Phys. B, 2023, 32 (**7**): 077102. DOI: 10.1088/1674-1056/aca7ef

## Flat band in hole-doped transition metal dichalcogenide observed by angle-resolved photoemission spectroscopy

Zilu Wang(王子禄), Haoyu Dong(董皓宇), Weichang Zhou(周伟昌), Zhihai Cheng(程志海), and Shancai Wang(王善才)

Chin. Phys. B, 2023, 32 (**6**): 067103. DOI: 10.1088/1674-1056/acc7f9

## Relevance of 3d multiplet structure in nickelate and cuprate superconductors

Mi Jiang(蒋密)

Chin. Phys. B, 2021, 30 (**10**): 107103. DOI: 10.1088/1674-1056/abf646

---

# Electronic structure of cuprate–nickelate infinite-layer heterostructure

Dachuan Chen(陈大川)[1,2], Paul Worm[3], Liang Si(司良)[4,3], Chunxiao Zhang(张春小)[5], Fenglin Deng(邓凤麟)[1], Peiheng Jiang(蒋沛恒)[1,†], and Zhicheng Zhong(钟志诚)[1,‡]

[1] *CAS Key Laboratory of Magnetic Materials and Devices & Zhejiang Province Key Laboratory of Magnetic Materials and Application Technology, Ningbo Institute of Materials Technology and Engineering, Chinese Academy of Sciences, Ningbo* 315201, *China*

[2] *College of Materials Science and Opto-Electronic Technology, University of Chinese Academy of Sciences, Beijing* 100049, *China*

[3] *Institut für Festkörperphysik, TU Wien, Vienna* 1040, *Austria*

[4] *School of Physics, Northwest University, Xi'an* 710127, *China*

[5] *School of Physics and Optoelectronic Engineering, Shandong University of Technology, Shandong* 250049, *China*

(Received 28 February 2023; revised manuscript received 5 May 2023; accepted manuscript online 9 May 2023)

The discovery of superconductivity in Sr/Ca-doped infinite-layer nickelates Nd(La)$NiO_2$ thin films inspired extensive experimental and theoretical research. However, research on the possibilities of enhanced critical temperature by interface heterostructure is still lacking. Due to the similarities of the crystal structure and band structure of infinite-layer nickelate $LaNiO_2$ and cuprate $CaCuO_2$, we investigate the crystal, electronic and magnetic properties of $LaNiO_2$:$CaCuO_2$ heterostructure using density functional theory and dynamical mean-field theory. Our theoretical results demonstrate that, even a very weak inter-layer $z$-direction bond is formed, an intrinsic charge transfer between Cu-3$d_{x^2-y^2}$ and Ni-3$d_{x^2-y^2}$ orbitals is obtained. The weak interlayer hopping between Cu and Ni leaves a parallel band contributed by Ni/Cu-3$d_{x^2-y^2}$ orbitals near the Fermi energy. Such an infinite-layer heterostructure with negligible interlayer interaction and robust charge transfer opens a new way for interface engineering and nickelate superconductors.

**Keywords:** nickelate superconductor, infinite-layer oxide, perovskite heterostructure

**PACS:** 71.20.–b, 74.70.–b, 75.70.Cn **DOI:** 10.1088/1674-1056/acd368

## 1. Introduction

Recently, the discovery of superconductivity in Sr-doped nickel oxide thin films, such as $Nd_{1-x}Sr_xNiO_2$,[1,2] $La_{1-x}(Sr, Ca)_xNiO_2$[3,4] and $Pr_{1-x}Sr_xNiO_2$,[5,6] ushers in the age of nickel-based superconductivity.[7–9] The way to synthesize these nickelate superconductors is topotactic reduction, the reagent $CaH_2$ plays the role of moving the apical oxygen in perovskite $RNiO_3$ out, then the infinite-layer $RNiO_2$ thin film with cuprate-like $Ni^{1+}$ ($3d^9$) valence state is fabricated. Unlike the bulk materials, thin film materials have the well-known interfacial freedom. The interface engineering in perovskite heterostructure can bring about rich physical phenomena, such as spin, charge, lattice, and orbitals control.[10–13] This manipulation is significantly related with the apical oxygen which acts as an interlayer bridge that connects the inter-layer d-orbitals, reshaping the orbital occupations, magnetic and electronic structures.[14–17] However, the apical oxygen in perovskite $ABO_3$ heterostructure is absent in infinite-layer. Thus, the opening questions are: (i) what is the difference between perovskite heterostructure and infinite-layer heterostructure, and (ii) will there be new interface physics in the infinite-layer nickelate and cuprate superconductors.

Here, we investigate the electronic structure and magnetic properties of infinite-layer heterostructure composed by $LaNiO_2$ (LNO) and its isostructural compound $CaCuO_2$ (CCO), and compare its electronic and magnetic properties with those of LNO and CCO through density functional theory plus Hubbard $U$ (DFT + $U$) calculations. We notice that the key characteristics of LNO and CCO, such as the self-doping effect,[7,18–22] La-5d and Ni-3d hybridizations,[23–26] competing magnetic phase[27] in LNO, d–p hybridization,[28] Emery picture,[29] in-plane antiferromagnetic coupling in CCO,[30–32] and most importantly the quasi-two-dimensional (2D) Ni/Cu-3$d_{x^2-y^2}$ band near crossing Fermi level ($E_f$), are preserved in $LaNiO_2$:$CaCuO_2$ heterostructure (LNO:CCO HS). The quasi-2D characters of 3$d_{x^2-y^2}$ band of Ni/Cu are reserved due to the negligible inter-layer hopping along the out-of-plane direction, leaving parallel 3$d_{x^2-y^2}$ band groups at $E_f$. However, an intrinsic charge transfer is induced by the potential difference between Cu-3d and Ni-3d. To consider the strong correlation effects in both Cu-3d and Ni-3d, electronic structures are computed using the dynamical mean-field theory (DMFT), the DFT observed parallel band structure of pure Cu-3$d_{x^2-y^2}$ and Ni-3$d_{x^2-y^2}$ states as well as the charge transfer effects are strongly renormalized under correlations. With the effective inter-layer doping effect induced by charge transfer between Ni and Cu, the heterostructure LNO:CCO interface is expected to host superconductivity without additional hole

†Corresponding author. E-mail: jiangph@nimte.ac.cn

‡Corresponding author. E-mail: zhong@nimte.ac.cn

© 2023 Chinese Physical Society and IOP Publishing Ltd 

doping. These features of infinite-layer heterostructure will offer new perspectives for understanding and tuning the superconductivity in nickelates.

## 2. Methods

### 2.1. DFT

We performed the DFT calculations within the generalized gradient approximation Perdew–Burke–Ernzerhof (GGA-PBE) functional and the projector augmented wave (PAW) method as implemented in the Vienna *ab initio* simulation package (VASP).[33–35] To avoid artificial results from different DFT codes, we also used the WIEN2K code with plane wave and full-electron potential method as double check. Structural relaxations were performed by spin-polarized calculations with ferromagnetic configuration to include spin splitting and magnetic effect. To include the electronic correlations, we used DFT + $U$ method with $U = 5.0$ eV for Ni-3d, $U = 5.0$ eV for Cu-3d and $U = 2.0$ eV for La-5d. The relaxed lattice constants were $a = b = 3.94$ Å and $c = 3.33$ Å for LNO, $a = b = 3.87$ Å and $c = 3.34$ Å for CCO, $a = b = 3.89$ Å and $c = 6.44$ Å for LNO:CCO HS, as shown in Fig. 1(a). To determine the magnetic ground state, we considered several possible magnetic orders, including typical ferromagnetic (FM) (0,0,0), G-type antiferromagnetic (AFM) ($\pi$,$\pi$,$\pi$) ($\sqrt{2} \times \sqrt{2} \times 1$ supercell), C-type AFM ($\pi$,$\pi$,0) ($\sqrt{2} \times \sqrt{2} \times 1$ supercell), and other complex configurations are shown in Fig. 1(b). To guarantee the convergence of calculations, the kinetic energy cut-off was set to 500 eV. The Brillouin zone was sampled with $13 \times 13 \times 15$ (bulk LNO and CCO), $13 \times 13 \times 8$ (LNO:CCO HS), and $8 \times 8 \times 12$ ($\sqrt{2} \times \sqrt{2} \times 1$ supercell) Monkhorst–Pack $k$-grids. For simplicity, we used the virtual crystal approximation (VCA) as implemented in VASP to simulate the doping cases.[36] In order to calculate the orbital occupations and analyze the intra- and inter-site hybridizations between each orbital, we projected La-5d and Ni/Cu-3d bands onto maximally localized Wannier functions[37] to obtain the tight-binding model Hamiltonian using WANNIER90 package[38] and have also been checked by WIEN2WANNIER interfaces.[39]

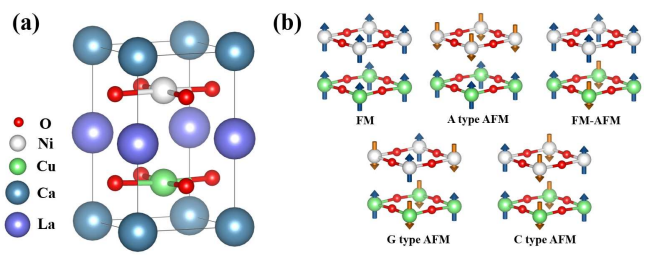



**Fig. 1.** (a) Crystal structure of LNO:CCO HS and (b) the corresponding magnetic configurations.

### 2.2. DMFT

The WIEN2K bands around the Fermi level are projected onto maximally localized Wannier functions and supplemented by local on-site Hubbard interaction $U = 3.2$ eV. Here, we project Wannier functions onto the Ni/Cu-3d$_{x^2-y^2}$ derived orbital that crosses the Fermi-surface in the $NiO_2$ and $CuO_2$ sheets. The low-energy effective Hamiltonian has subsequently been solved within DMFT at $\beta = 38.68$ eV using continuous-time quantum Monte Carlo simulations in the hybridization expansions[40] implemented in W2DYNAMICS.[41,42] The maximum entropy method[43,44] is employed for an analytic continuation of the spectra.

## 3. Results

### 3.1. Electronic structure

First, we calculate the orbital projected electronic structure and the projected density of states (PDOS) of LNO:CCO HS and their counterparts, LNO and CCO, by DFT + $U$ method. As shown in Fig. 2(a), CCO displays the single band feature in its band structure, specifically contributed by 3d$_{x^2-y^2}$ band of Cu, which is the starting point of the cuprate superconductivity theoretical mechanism.[45–47] As the PDOS of CCO shows, the energy dispersion of Cu-3d$_{x^2-y^2}$ ranges from $-1$ eV to 2 eV, and part of them hybridizes with O-p orbitals as shown in the range of $-1$ eV to $-3$ eV. In Fig. 2(b), LNO exhibits roughly two different band characteristics from CCO. One is the larger energy splitting between Ni-3d$_{x^2-y^2}$ and O-p orbitals, as shown in Fig. 2(b). Such difference is the typical characters of cuprate charge-transfer insulator[48] ($U > \Delta$: $\Delta$ is the charge transfer energy) and nickelate Hubbard system[49] ($U < \Delta$). Another feature of nickelate is the overlap between La-5d and Ni-3d orbitals. The La-5d$_{z^2}$ and La-5d$_{xy}$ bands, which are represented by red dots in Fig. 2(b), cross the $E_f$, leading to electron occupation in La-5d. This occupation results in the so-called self-doping effect, and also gives rise to the discussion on single- vs. multi-band model debates,[18–21,50] however, the current experimental and theoretical results evidence the effectiveness of single-band model in nickelate $ANiO_2$ superconductors.[22–24] Therefore, the opening question is whether such self-doping effect in LNO:CCO HS is reserved, and do other d bands need to be taken into account in the minimized model? To answer this we next investigate the electronic structure of LNO:CCO system.

Figure 2(c) depicts the band structure of LNO:CCO HS, we can see that the parallel bands near the Fermi level are formed. Through the orbital projection and PDOS analysis, we find that the energetically higher band is from Ni-3d$_{x^2-y^2}$ orbital while the lower band is from Cu-3d$_{x^2-y^2}$ orbital. For the Ni-3d$_{x^2-y^2}$ band, there exists a self-doping effect due to the overlap between La-5d bands and Ni-3d bands at $M$-point. The

energy gap between Ni-3d$_{x^2-y^2}$ and O-p is 2.76 eV. As for the Cu-3d$_{x^2-y^2}$ band, the hybridization between Cu-3d$_{x^2-y^2}$ and O-p orbitals becomes weaker than that in CCO, which is obviously evidenced by comparing the DOS of LNO:CCO HS and CCO bulk in Fig. 2(a), leading to a rather pure 3d$_{x^2-y^2}$ state band near $E_f$. Thus, the main features of LNO and CCO are maintained in LNO:CCO HS, and a parallel band structure is formed at $E_f$. To investigate the hybridization of the parallel band, we project Ni/Cu-3d$_{x^2-y^2}$ bands onto maximally localized Wannier functions. The obtained hopping terms between Ni and Cu are close to zero ($t = 0.05$, the corresponding Wannier function is shown in Fig. S1), suggesting these two quasi-2D bands are weakly hybridized. We also find the PDOS peak of Ni-3d$_{x^2-y^2}$ rises from $-0.4$ eV in LNO to 0.1 eV in the heterostructure, and the PDOS peak of Cu-3d$_{x^2-y^2}$ drops off observably, indicating an intrinsic charge transfer from Ni to Cu.

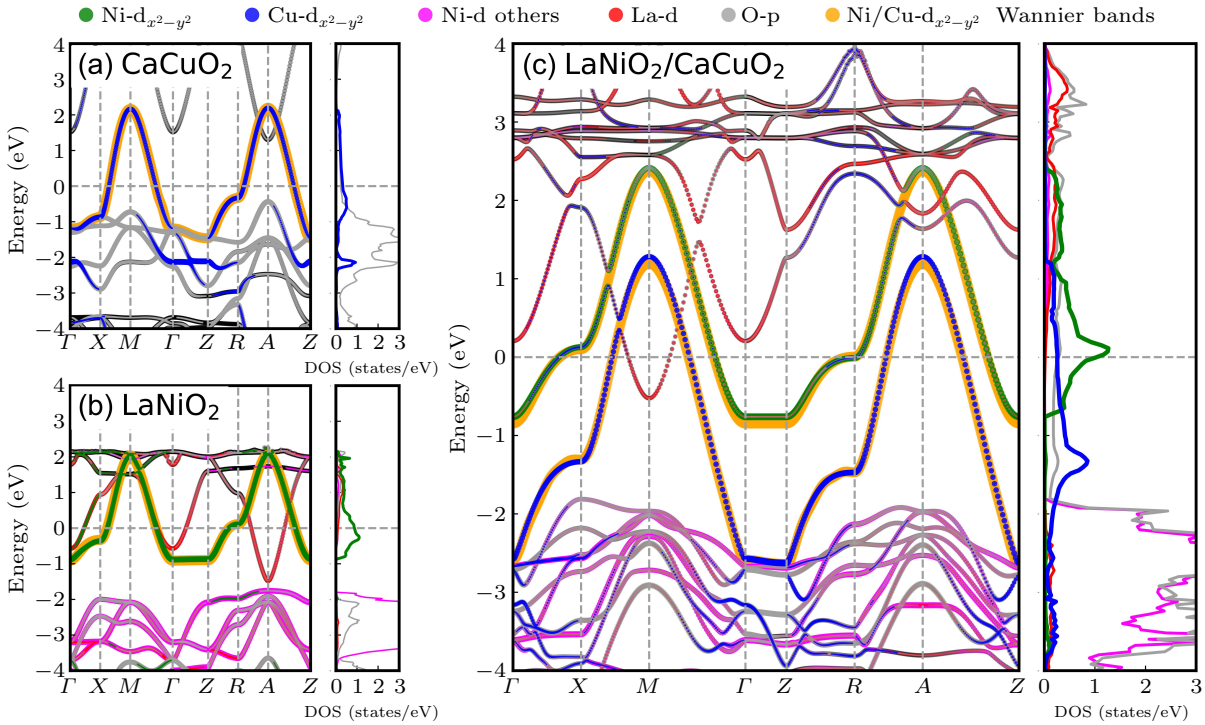



**Fig. 2.** Orbital projected electronic band structures of (a) bulk CCO, (b) bulk LNO and (c) LNO:CCO HS. The corresponding Wannier projected bands are shown by orange dots, and the projected density of states is on the right side of each band structure.

### 3.2. Charge transfer

To investigate the driving force of the charge transfer and self-doping effect in LNO:CCO HS, we first check the relevance of charge transfer to the $U$ interaction. As shown in Figs. S2 and S3, with the increase of $U$ (from 0 eV to 6 eV), the others Ni/Cu-3d orbital and O-p orbital bands energetically shift down by $\sim$ 1.3 eV, the parallel band's structure near $E_f$ is reserved. Moreover, the band gap between Ni-3d$_{x^2-y^2}$ and Cu-3d$_{x^2-y^2}$ slightly increases from $\sim$ 1.0 eV ($U = 0$ eV) to $\sim$ 1.5 eV ($U = 6$ eV), demonstrating larger charge transfer at larger $U$. So that the charge transfer is significant no matter $U$ is large or small and it only varies slightly under different value of $U$, which indicates that the driving force of charge transfer effect can not be simply attributed to Hubbard interaction. Another possible way to modify this charge transfer is the substrate strain. As shown in Fig. S4, we simulate the in-plane strain in an experimentally reasonable region of $-5\%$ to 5%. With increasing strain, the parallel band barely moved, meaning the charge transfer is not suppressed obviously. In a word, we propose that the interface of LNO:CCO induces a robust charge transfer between Ni-3d$_{x^2-y^2}$ and Cu-3d$_{x^2-y^2}$ orbitals.

In order to estimate the amount of the transferred charge, we performed the Wannier projection to calculate their occupations.[51] The calculated tight-binding hopping parameters of the parallel bands are $-0.39$ eV and $-0.44$ eV for the nearest-neighbor ($\boldsymbol{R}_{100/010}$) hopping of Ni and Cu-3d$_{x^2-y^2}$ orbitals, respectively, the second nearest-neighbor ($\boldsymbol{R}_{110}$) hopping parameters are 0.10 eV for both Ni and Cu, and the on-site hopping ($\boldsymbol{R}_{000}$) energy are 7.93 eV for Ni and 6.70 eV for Cu. Based on these tight-binding model Hamiltonian, we computed the occupations at Ni/Cu-3d$_{x^2-y^2}$ orbitals by integrating the DOS of Wannier bands. We denoted the occupied electrons of band Ni-3d$_{x^2-y^2}$ as $n_1$ and Cu-3d$_{x^2-y^2}$ as $n_2$. Figures 3(a) and 3(b) show the computed occupation number of Ni-3d$_{x^2-y^2}$ is 0.58 and Cu-3d$_{x^2-y^2}$ is 1.40 in LNO:CCO HS. Due to the omission of the distribution of d–p hybridization part (below $-2.5$ eV as shown in Fig. 2(a) PDOS), 1.40 electrons at Cu-

$3d_{x^2-y^2}$ might be overestimated. The orange lines in Figs. 3(a) and 3(b) show the function between doping concentrations and $n_1/n_2$ in LNO and CCO, respectively. In undoped LNO, $n_1$ is 0.78, which is close to the previous DFT results,[51] and $n_2$ is $\sim 0.97$ in parent CCO. Therefore, the LNO:CCO HS can be described by a two non-hybridrized parallel band structure model with electronegativity-induced charge transfer, which is about 0.20 per Ni to Cu.

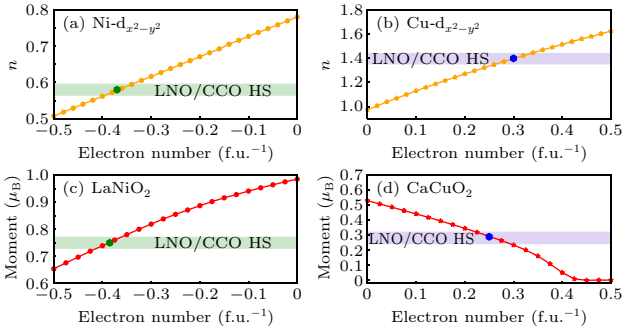



**Fig. 3.** The function between doping concentrations and occupation number of $3d_{x^2-y^2}$ orbital in (a) LNO and (b) CCO calculated by Wannier bands, the electron and hole doping are represented by positive and negative doped electrons, respectively. The magnetic moment of Ni/Cu in the ground state (c) LNO (FM) and (d) CCO (AFM) at different doping concentrations. The green and blue hexagons represent the occupation and moment of Ni and Cu in LNO:CCO HS, respectively.

### 3.3. Magnetism

We next study the magnetic properties of LNO:CCO HS using DFT + $U$ method. The DFT calculations indicate that the magnetic ground state of LNO and CCO is very sensitive to the doping. The parent cuprate is a stable G- or C-type AFM order while the intra-layer AFM coupling can be suppressed by either electron or hole doping. Due to the competing magnetic phase in nickelate, the FM interaction will be enhanced by hole doping,[27] meanwhile, the AFM order is stable in weakly electron doped CCO. Based on the above facts, we hence predict that the LNO:CCO HS with inter-layer Ni–Cu charge transfer will converge to FM-AFM state, which is composed by hole doped LNO layer and electron doped CCO layer.

To confirm this we computed the total energies of different possible magnetic states of LNO:CCO HS, the results are summarized in Table 1. The most stable magnetic order is FM-AFM, which represents the FM in LNO layer and AFM in CCO layer. The calculated magnetic moment of Ni and Cu is $0.75\mu_B$ and $0.29\mu_B$, respectively. The small magnetic moment at Cu is resulted from that in CCO layer parts the moment is mainly located at O sites due to the Cu–O d–p hybridization. Additionally, as mentioned above, the estimated $n_1$ and $n_2$ in LNO:CCO HS is 0.58 and 1.40, i,e., the filling at Cu-$3d_{x^2-y^2}$ is larger than half-filling, the externally doped electrons also play a role in reducing its moment. We calculate the corresponding magnetic moment in LNO and CCO through DFT + $U$ method as shown in Figs. 3(c) and 3(d) with $n_1 = 0.58$ (effectively 0.37 f.u.$^{-1}$ hole doped in LNO) and $n_2 = 1.40$ (effectively 0.30 f.u.$^{-1}$ electron doped in CCO), the corresponding moment is about $0.76\mu_B$ for Ni and $0.22\mu_B$ for Cu. These two estimated values are close to the DFT calculated values in Table 1, which indicates that the magnetic properties of LNO:CCO HS can be approximated as a combination of LNO and CCO. This conclusion is confirmed by plenty of facts. For example, the moment of Cu in FM and A-type AFM is close to zero, suggesting the FM in CCO layer can not be stabilized, which is consistent with the electron doped CCO.[26] Meanwhile, the energy difference between AFM and NM is small when the electron concentrations increase in CCO,[27] and the energy different between FM and FM-AFM in LNO:CCO HS is only 15 meV. Comparing the energy of G-type AFM and C-type AFM, the energy difference is 9 meV, so we deduce that the magnetic interaction between Cu and Ni is neglectable. Figure 4 shows the PDOS of the magnetic ground state of LNO:CCO HS, and that of LNO and CCO with the same occupation number in Ni/Cu-$3d_{x^2-y^2}$ orbitals. Focus on Fig. 4(a), we notice that the FM magnetic moment is contributed by Ni-$3d_{x^2-y^2}$ orbital, and the AFM magnetic moment is contributed

**Table 1.** The total energy and magnetic moment of different magnetic orders (refer to Fig. 1), the energy of non-magnetic state is set to zero.

| Type | FM | A-type AFM | FM-AFM | G-type AFM | C-type AFM |
|---|---|---|---|---|---|
| Energy (meV) | −447 | −447 | −464 | −259 | −250 |
| Moment ($\mu_B$/Ni) | 0.71 | 0.71 | 0.75 | 0.76 | 0.74 |
| Moment ($\mu_B$/Cu) | 0.02 | 0.02 | 0.29 | 0.39 | 0.37 |

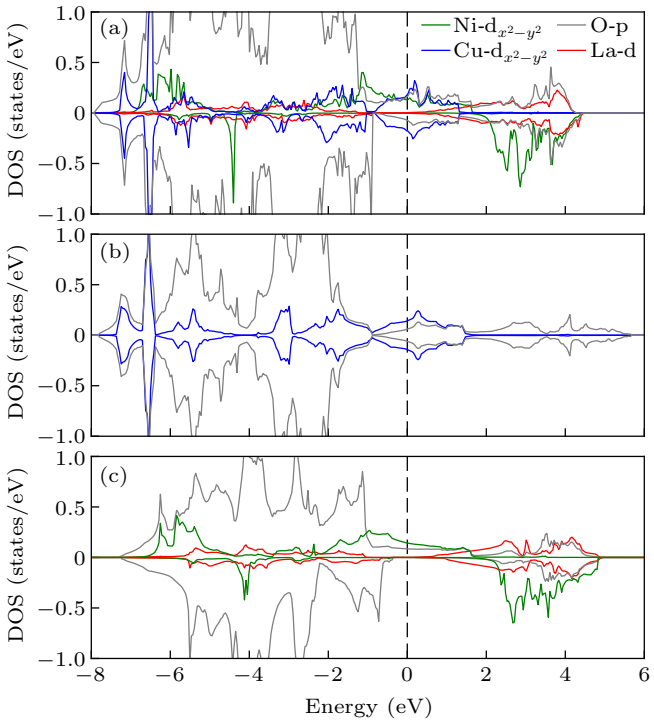



**Fig. 4.** The projected density of states for (a) FM-AFM LNO:CCO HS, (b) AFM CCO with 0.30 electron doping per Cu, and (c) FM LNO with 0.37 hole doping per Ni.

by Cu-3d$_{x^2-y^2}$ orbital, this is consistent with LNO and CCO as shown in Figs. 4(b) and 4(c). It can be approximated thought that the PDOS of FM-AFM LNO:CCO HS is a superposition of FM LNO and AFM CCO, which indicates that the magnetic properties of each layer block in LNO:CCO HS are preserved, and the magnetic interaction in $z$ direction is weak.

### 3.4. Robust parallel bands under correlation

We compute the DMFT $k$-resolved spectral function and display it along a high-symmetry path in the Brillouin zone together with the DFT bands (white lines) as shown in Fig. 5(a). One can readily observe two features. First, we can notice a charge transfer, which partially counteracts the values predicted by DFT. That is, 0.13 electrons relocate back from the copper site to the nickel orbital, which makes a total occupation at Ni of 0.78 and 1.22 at copper. The Fermi surface is displayed in Fig. 5(c), with blue and red lines for the Ni and Cu sites, respectively. Aside from the different occupations, one can also readily see the slightly larger $k_z$ dispersion in Ni, which has already been reported previously.[52] Secondly, the bands are renormalized due to the onsite interaction and display lower and upper Hubbard bands, visible in the $k$-integrated spectral function at $\pm 3.2$ eV. Together with this on-site interaction drove renormalization, an increase in the effective mass $m^*/m$ of 2.4 for Ni and 1.8 for Cu also comes.

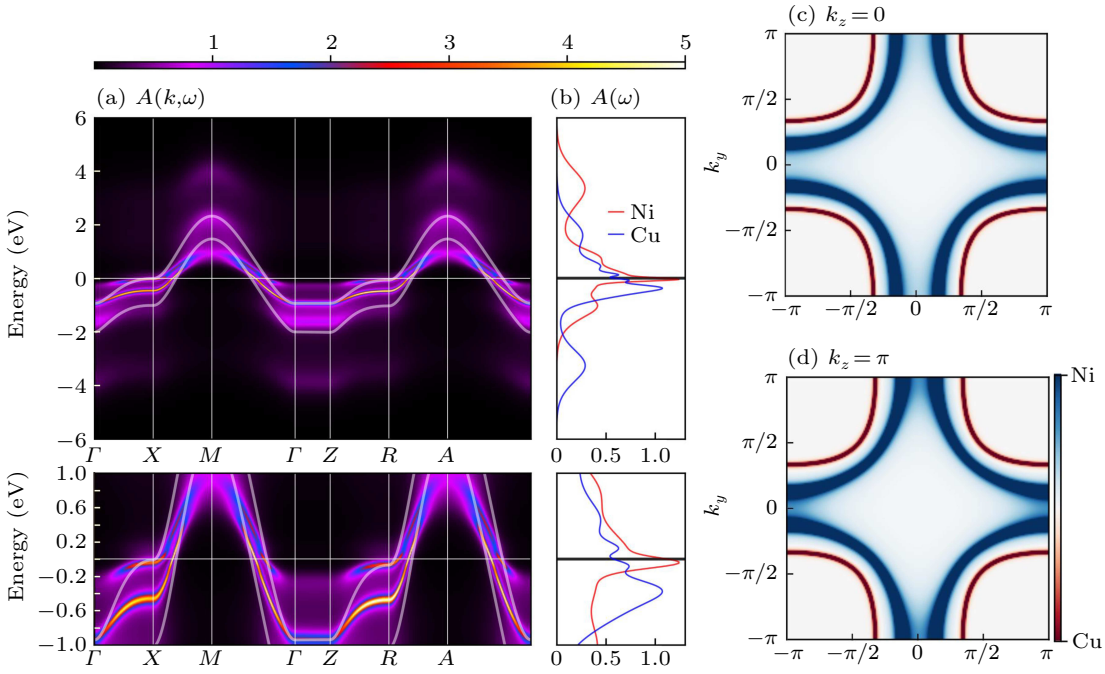



**Fig. 5.** (a) DMFT spectral function $A(k,\omega)$ and (b) $k$-integrated spectral function $A(\omega)$, bottom shows a zoom in around the Fermi surface. Panels (c) and (d) are Fermi surface as obtained by DMFT at $k_z = 0$ and $k_z = \pi$. Blue marks the nickel orbital, while red is for copper.

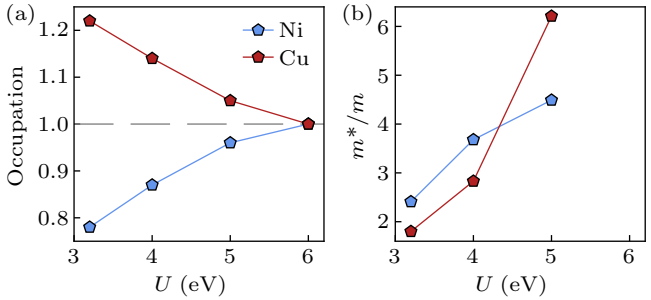



**Fig. 6.** Evolution of the (a) occupation and (b) effective mass with the interaction value $U$. Between $U = 5$ eV and 6 eV the system undergoes a Mott metal to insulator transition.

Here, we discuss the evolution of the system with increasing on-site coulomb interaction $U$. For simplicity we restrict ourselves to the case where the on-site Coulomb interaction is the same on the Ni and Cu sites. In Fig. 6, we show occupation and effective mass as a function of interaction value $U$. Let us note that the system undergoes a Mott metal to insulator transition between $U = 5$ eV and 6 eV. In the Mott insulating state, both sites have equal occupation of one electron per Ni/Cu orbital and infinite effective mass. As already discussed above, we observe a charge transfer that restores half filling for both sites when the Mott insulating phase is reached. Here it seems the transfer is simply linear in $U$. The effective mass increases with increasing interaction, which is generally to be expected. However, we note that for lower interaction values, the Ni site is more correlated, while this is reversed at higher ones.

## 4. Discussion and conclusion

Benefiting from the discovery of infinite-layer nickelate superconductors, interface engineering with infinite-layer structure will offer new opportunities for HS design. Taking LNO:CCO HS as an example, we perform the DFT + DMFT

methods to systematically study the features of LNO:CCO HS. Through electronic and magnetic analysis, we notice that the characteristics of two different layers, such as d–p hybridization in CCO layer and self-doping bands in LNO layer are preserved in the LNO:CCO HS. The magnetic properties of intralayer cuprate and nickelate are also retained in their HS due to the disappearance of interlayer super-exchange interaction. A pure parallel band contributed by Ni/Cu-3d$_{x^2-y^2}$ orbitals with a charge transfer is found. In conclusion, we highlight that the intrinsic doping in infinite-layer HS induced by charge transfer can control the concentration in each layer without the breaking of the original electronic and magnetic properties of its counterparts. This work opens a new way for interface design in infinite-layer LNO:CCO HS.

## Acknowledgments

Project supported by the National Key Research and Development Program of China (Grant Nos. 2021YFA0718900 and 2022YFA1403000), the Key Research Program of Frontier Sciences of CAS (Grant No. ZDBS-LY-SLH008), the National Natural Science Foundation of China (Grant Nos. 11974365, 12004400, and 51931011), the Science Center of the National Natural Science Foundation of China (Grant No. 52088101), and the K. C. Wong Education Foundation (Grant No. GJTD-2020-11). Calculations were performed at the Supercomputing Center of Ningbo Institute of Materials Technology and Engineering and Vienna Scientific Clusters (VSC).

## References

[1] Li D, Lee K, Wang B Y, *et al.* 2019 *Nature* **572** 624
[2] Zeng S, Yin X, Li C, *et al.* 2022 *Nat. Commun.* **13** 743
[3] Osada M, Wang B Y, Goodge B H, *et al.* 2021 *Adv. Mater.* **33** 2104083
[4] Zeng S, Li C, Chow L E, *et al.* 2022 *Sci. Adv.* **8** eabl9927
[5] Osada M, Wang B Y, Goodge B H, *et al.* 2020 *Nano Lett.* **20** 5735
[6] Osada M, Wang B Y, Lee K, *et al.* 2020 *Phys. Rev. Mater.* **4** 121801
[7] Gu Q and Wen H 2022 *Innovation* **3** 100202
[8] Zhang J and Tao X 2021 *CrystEngComm* **23** 3249
[9] Nomura Y and Arita R 2022 *Rep. Prog. Phys.* **85** 052501
[10] Tokura Y and Nagaosa N 2000 *Science* **288** 462
[11] Poeppelmeier K R and Rondinelli J M 2016 *Nat. Chem.* **8** 292
[12] Dagotto E, Hotta T and Moreo A 2001 *Phys. Rep.* **344** 1
[13] Chakhalian J, Freeland J, Habermeier H U, *et al.* 2007 *Science* **318** 1114
[14] Hansmann P, Yang X, Toschi A, *et al.* 2009 *Phys. Rev. Lett.* **103** 016401
[15] Catalano S, Gibert M, Fowlie J, *et al.* 2018 *Rep. Prog. Phys.* **81** 046501
[16] Chakhalian J, Freeland J W, Millis A J, *et al.* 2014 *Rev. Mod. Phys.* **86** 1189
[17] Chen X, Zhang S, Liu B, *et al.* 2021 *Phys. Rev. B* **104** 045310
[18] Lee K W and Pickett W 2004 *Phys. Rev. B* **70** 165109
[19] Karp J, Botana A S, Norman M R, *et al.* 2020 *Phys. Rev. X* **10** 021061
[20] Been E, Lee W S, Hwang H Y, *et al.* 2021 *Phys. Rev. X* **11** 011050
[21] Kapeghian J and Botana A S 2020 *Phys. Rev. B* **102** 205130
[22] Jiang P, Si L, Liao Z, *et al.* 2019 *Phys. Rev. B* **100** 201106
[23] Yang Y F and Zhang G M 2022 *Front. Phys.* **9** 783
[24] Zhang G M, Yang Y F and Zhang F C 2020 *Phys. Rev. B* **101** 020501
[25] Gu Y, Zhu S, Wang X, *et al.* 2020 *Commun. Phys.* **3** 84
[26] Zhang M, Zhang Y, Guo H M, *et al.* 2021 *Chin. Phys. B* **30** 108204
[27] Chen D, Jiang P, Si L, *et al.* 2022 *Phys. Rev. B* **106** 045105
[28] Hybertsen M S, Stechel E, Schluter M, *et al.* 1990 *Phys. Rev. B* **41** 11068
[29] Fischer M H and Kim E A 2011 *Phys. Rev. B* **84** 144502
[30] Vaknin D, Sinha S, Moncton D, *et al.* 1987 *Phys. Rev. Lett.* **58** 2802
[31] Pickett W E 1989 *Rev. Mod. Phys.* **61** 433
[32] Armitage N, Fournier P and Greene R 2010 *Rev. Mod. Phys.* **82** 2421
[33] Kresse G and Furthmüller J 1996 *Comput. Mater. Sci.* **6** 15
[34] Kresse G and Furthmüller J 1996 *Phys. Rev. B* **54** 11169
[35] Perdew J P, Burke K and Ernzerhof M 1996 *Phys. Rev. Lett.* **77** 3865
[36] Bellaiche L and Vanderbilt D 2000 *Phys. Rev. B* **61** 7877
[37] Wannier G H 1937 *Phys. Rev.* **52** 191
[38] Pizzi G, Vitale V, Arita R, *et al.* 2020 *J. Phys. Condens. Matter* **32** 165902
[39] Kuneš J, Arita R, Wissgott P, *et al.* 2010 *Comput. Phys. Commun.* **181** 1888
[40] Gull E, Millis A J, Lichtenstein A I, *et al.* 2011 *Rev. Mod. Phys.* **83** 349
[41] Wallerberger M, Hausoel A, Gunacker P, *et al.* 2019 *Comput. Phys. Commun.* **235** 388
[42] Parragh N, Toschi A, Held K, *et al.* 2012 *Phys. Rev. B* **86** 155158
[43] Sandvik A W 1998 *Phys. Rev. B* **57** 10287
[44] Gubernatis J, Jarrell M, Silver R, *et al.* 1991 *Phys. Rev. B* **44** 6011
[45] Anderson P W 1987 *Science* **235** 1196
[46] Gull E and Millis A 2015 *Nat. Phys.* **11** 808
[47] Jiang H C and Devereaux T P 2019 *Science* **365** 1424
[48] Zaanen J, Sawatzky G and Allen J 1985 *Phys. Rev. Lett.* **55** 418
[49] Goodge B H, Li D, Lee K, *et al.* 2021 *Proc. Natl. Acad. Sci. USA* **118** e2007683118
[50] Jiang M 2021 *Chin. Phys. B* **30** 107103
[51] Deng F, Jiang P, Lu Y, *et al.* 2021 *Europhys. Lett.* **135** 67001
[52] Kitatani M, Si L, Janson O, *et al.* 2020 *npj Quantum Mater.* **5** 59